Molecular dynamics simulations of non-equilibrium systems

Nordlund, Kai Henrik

Springer International Publishing AG
2020

Nordlund , K H & Djurabekova , F G 2020 , Molecular dynamics simulations of non-equilibrium systems . in W Andreoni & S Yip (eds) , Handbook of materials modeling : Applications: Current and Emerging Materials . 2nd edn , Springer International Publishing AG , Cham , pp. 2161-2192 . https://doi.org/10.1007/978-3-319-44680-6_119

http://hdl.handle.net/10138/342325
https://doi.org/10.1007/978-3-319-44680-6_119

acceptedVersion

Preprint of paper published in Handbook of Materials Modelling

Molecular Dynamics simulations of non-equilibrium systems

Flyura Djurabekova and Kai Nordlund

Abstract The materials in nuclear reactors are subject to several radiation damage mechanisms. High-energy neutrons can give high (keV) recoil energies to nuclei via elastic collisions, many different nuclear reactions can also lead to lower recoil energies to nuclei, and nuclear fission fragments can get MeV kinetic energies from the fission process. The nuclei with high kinetic energies can damage the material both via nuclear and electronic excitations. In this Article, we first overview briefly the nuclear damage mechanisms, then discuss how molecular dynamics methods can be used to model the ensuing damage, both in the nuclear and electronic collision regimes. Some examples of recent results from both the nuclear and electronic regime are provided in the end.

1 Introduction

Nuclear reactor systems involve a large number of non-equilibrium effects that can affect the materials in the reactors. The neutrons coming from a fission or fusion reactor can damage materials in many ways. When they have high (MeV) energies, they will occasionally collide strongly with nuclei in the materials, and transfer a high amount of energy to these. The maximum energy can easily be estimated from the classical kinematics equation of energy transfer between particles of masses m_1 and m_2 in a head-on collision:

$$E_{transferred} = \frac{4m_1m_2}{(m_1+m_2)^2}E_{initial} \tag{1}$$

Flyura Djurabekova and Kai Nordlund
Department of Physics and Helsinki Institute of Physics, University of Helsinki, PB 43, 00014 University of Helsinki, Finland, e-mail: flyura.djurabekova@helsinki.fi

For e.g. a neutron energy of 2 MeV moving in Cu, this amounts to a maximum energy transfer of about 120 keV. More accurate calculations considering that not all collisions are head-on, show that the typical transferred energies are lower, but still tens of keV's (Averback and Diaz de la Rubia 1998). These energies are about four orders of magnitude higher than the cohesive energy of the material, making it clear that they can lead to considerable damage in the materials. The atomic collisions induced by such high-energy ions are known as collision cascades, and the slowing down by these collisions as *nuclear stopping*.

Also neutrons at lower energies can lead to damage in the materials. Damage production by the direct collision mechanism is possible down to energies of the minimum threshold displacement energy (Nordlund et al 2005) of the material, i.e. neutron energies of a few hundred eV. When the neutron is thermalized to even lower energies, it will eventually undergo a nuclear reaction. These reactions almost always lead to another recoil energy. For instance, in (n,γ) reactions the emitted γ particle has enough momentum to give the nucleus a recoil energy of a few hundred eV, enough for damage production (Raman et al 1994). Naturally, if the emitted particle has a mass, such as in (n,α) reactions, the energy transfer is even higher, and also the emitted massive particle can cause damage.

Finally, if the neutron causes a fission reaction, the fission fragments can have energies of hundreds of MeV's (note that this energy release is the origin of energy production in normal nuclear power plants). At these very high energies, the fission fragments slow down mainly by collisions with electrons, known as *electronic stopping* (Ziegler et al 1985). On the other hand, the nuclear collision energy transfer is much reduced at these high energies, and hence the electronic stopping dominates the energy loss. Heavy ions that slow down mainly by the electronic stopping are commonly called swift heavy ions. This interaction excites a large number of electrons into the conduction band. Since the energy loss to electrons does not alter the path of the ion appreciably, the swift heavy ions move in straight paths, and the damage they produced is in straight cylindrical regions called ion tracks (Lang et al 2008) . De-excitation of the excited electrons in the insulating materials takes place within the limited region around the ion track. The released energy can then be transferred to the atoms in the lattice, known as "electron-phonon" coupling, leading to damage production. This damage can be produced via different atomic-level mechanisms.

Naturally, both mechanisms of damage production either in collision cascades or by swift heavy ion (via nuclear or electronic stopping powers, respectively) are relevant also in other systems. Ion implantation is a routinely used approach to dope silicon in the semiconductor industry, and the ions induce collision cascades that produce damage with mechanisms very similar to the neutron-induced ones (Chason et al 1997). Ion tracks, on the other hand, are also naturally present in many minerals, produced in these by fission fragments from radioactive decay. The density of these is used routinely as a dating technique (Gallagher et al 1998). They can also be produced deliberately by high-energy particle accelerators, and are a basis of many promising nanoscience applications (Apel 2003; M. E. Toimil-Molares 2012). Such

very high-energy particles are also present in space, and can be a serious issue for reliability of electronics in space (Fleetwood et al 1994).

Experimentally, the radiation damage can be detected in many different ways, and we mention here only a few key methods. As collision cascades only exist for a few ps, the atom motion in them cannot be directly detected. However, there is a special nuclear approach that has been used to determine the lifetime of a cascade in Fe to be 6 ps (Stuchbery and Bezakova 1999). Transmission electron microscopy (TEM) observation of amorphous pockets in semiconductors (Ruault et al 1984; Bench et al 2000) and local phase transitions in ceramics (Meldrum et al 1998) also provide compelling evidence of dense regions of collision associated with the nuclear stopping. Moreover, field ion microscopy experiments have shown that 20-30 keV heavy ion irradiation can lead to dense regions of vacancies in W (Current et al 1983) and more recent transmission electron microscopy has shown that 150 keV W cascades can directly produce dislocation loops in this material (Yi et al 2015).

Ion tracks can also be detected experimentally in many different ways. In initially crystalline materials, chemical etching can reveal the location and areal density of tracks, since the damage track core etches faster than perfect crystal (Skupinski et al 2005). However, this method does not tell anything about the atomic structure of the tracks. Cross-sectional TEM can be used to image tracks on the atomic level, either from the sides are as a cross section. TEM experiments have shown that the core of a track is amorphous (Meftah et al 1994b; Toulemonde et al 2006). Rather recently, small-angle x-ray scattering experiments have revealed that the core of an ion track is underdense (Kluth et al 2008).

In this Chapter, we focus on computational methods for collision cascades and ion tracks, with some emphasis on new developments during the last ten years. We review the methods of atomistic simulations of such high-energy irradiation effects relevant in nuclear systems, both in the nuclear collision and swift heavy ion regimes. In both cases, standard molecular dynamics simulation approaches will not work directly, since the high kinetic energies involved may lead to serious energy nonconservation issues.

2 Modelling approaches

The computer simulation approaches, developed to simulate materials in out-of-equilibrium conditions, are similar to those used for thermodynamically equilibrated systems. The latter, however, must be adjusted to capture the physics of processes taking place under irradiation with energetic ions. Every energetic ion passing through the surface, transfers the energy and the momentum to the atoms of the irradiated material in a cascade until all the energy, which was brought in by the ion, dissipates inside the material. A prolonged ion irradiation with a high fluence (number of ions arriving at a unit surface during the entire irradiation time) may cause appreciable damage, however, the experimental rates – ion fluxes given by

the number of ions per unit surface per unit time – are usually very low. The actual time interval between two subsequent cascades is much longer than the duration of a single cascade, and hence, any temporal (and/or spatial) overlap of the cascades is routinely neglected. If the fluxes are very high, and the subsequent ion arrives at the surface while the previous cascade is still not extinguished, the temporal and spatial overlap of simultaneous multiple cascades may lead to strong non-linear effects. This situation is common during arc plasma-surface interaction Timkó et al (2010); Djurabekova et al (2012) and needs to be taken a special care by adjusting the size of the simulation box. However, in this chapter we will not consider the dense ion fluxes, but rather focus on individual cascades, which can be simulated one at a time. Bearing in mind that the size of a single cascade depends on the energy of an ion, the size of the simulation box can also be selected by using a simple empirical expression

$$N_{at} = 20 \cdot \frac{E_{kin}}{1eV} \tag{2}$$

This expression guarantees that the energy can be absorbed by the simulation box and dissipated gradually in a quasi-microcanonical ensemble. The latter requires additional clarification.

If a system of atoms is in a thermodynamic equilibrium, the properties of such a system can be described as averages of different thermodynamic ensembles (Allen and Tildesley 1989), depending on the property of interest. By fixing different external conditions, one can consider the micro-canonical (*NVE*) ensemble of an isolated system with the fixed number of atoms, N, within the fixed volume, V; the canonical (*NVT*) ensemble, connected to a heat bath of temperature T; and the isobaric-isothermal ensemble (*NPT*), which is connected to the heat bath and the volume of the system is flexible to keep the pressure P at a given value.

The control of temperature or pressure affects the velocities of the atoms. If baro- and thermostats are used during irradiation event simulations, the atom trajectories are perturbed from the true ones. For a cascade to be simulated properly, one has to allow a natural evolution of energy exchange in the system. In reality, the heat generated in the system during the development of the cascade, will dissipate through the heat conduction to the bulk outside the actual cascade region. However, as it was mentioned in the previous paragraph, the system to simulate a single cascade is not large enough to dissipate all the energy and, if applying a fully *NVE* ensemble in the simulations, the system will inevitably heat up. This is an artefact, which may affect the results of the cascade. To avoid it, an emulation of thermal conduction can be used, i.e. the side atoms outside of a cascade region can be connected to a heat bath, providing a channel for energy dissipation in a reasonable manner, removing the energy from the system, but not interfering with the atoms, which were directly involved in the cascade. We call such an ensemble quasi-microcanonical, since the energy is not fully conserved, although no scaling of the atom velocities is performed in the actual cascade simulations zone.

Thus far, two basic atomistic approaches have been used to simulate irradiation effects in large scale systems with the considerable number of atoms, binary collision approximation (BCA) and molecular dynamics (MD). Both approaches employ

the Born-Oppenheimer approximation, which allows separating nuclear and electronic subsystems and taking into consideration the large difference in the time- and size domains of both subsystems. In this approximation, the equations of motion are applied only to the massive and heavy nuclei, while the electrons follow the former immediately. This simplifies the simulation task and the atoms in this approximation can be considered as spherical objects interacting between themselves according to the forces. The latter are derived from potential functions, which are described in greater detail in subsection 3.

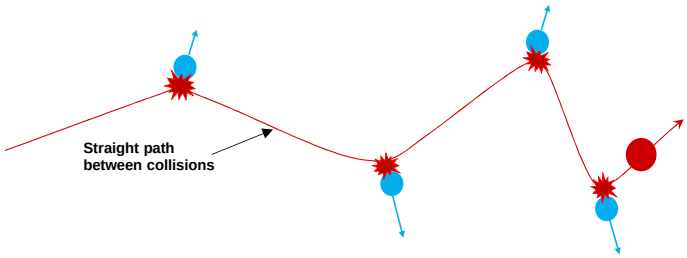

Fig. 1 Illustration of collisions in the binary collision approximation. Note that the other atoms, which are located near the knocked-on atoms, are not taken into account

Both BCA and MD were developed initially to simulate the materials in two different limits. The BCA approach describes the radiation effects in materials, i.e. it follows the trajectory of energetic projectile (either the ion, which entered the material or the recoil atom, which received the energy in a cascade) and calculates collision of this projectile and the encountered atom of the material at each BCA step (see Figure 1). BCA is designed to describe the short-range interactions, i.e. at the distances between the colliding particles which are too short to be affected by the other atoms in the material, so the collision is strictly binary and the interaction is only repulsive. Since the BCA calculates the collision between two particles at each simulation step, the simulations are very fast and do not require large computational capacity. There exist many codes developed by different groups, which either use a so-called “magic formula” replacing the exact solution of the collisional integral for the universal ZBL potential at every BCA step (Ziegler ????; Pugacheva et al 1998), or precalculate all the scattering angles for each projectile-atom pair in the system in advance and tabulate them as the function of impact parameter (Miyagawa et al 2002). However, the BCA approximation is not valid at low energies; already at the energies around 500 eV, the multi-body interactions between the atoms become important and determine the dynamics of defect formation. Also the BCA approach is working well for linear cascades: the interaction between a projectile (energetic particle) and the particle in rest. Strictly speaking, the particle-in-rest may be involved in thermal motion, which is much less intense compared to the motion of the projectile particle. In the dense

cascades, when many atoms are involved in the energy dissipation process (dense materials, such as metals of heavy elements), the interaction may happen between both moving atoms which leads to non-linear cascades or thermal spikes, where the application of BCA becomes questionable.

The MD method, on the other hand, was originally developed to describe the materials in thermodynamic ensembles. Generally speaking, the MD method solves the system of Newton?s equations, with the driving forces derived from the potential. In other words, the interatomic potential for the material of interest is the key function, which defines the accuracy of the MD simulations. Very careful attention is usually paid to develop a potential, which is able to reproduce certain properties, which the material exhibits in thermodynamic equilibrium conditions. If the potential is able to reproduce all or some properties of materials, such as crystal structure(s), lattice parameter, cohesive energy, melting and boiling temperatures, elastic moduli, Young's and shear moduli, etc., the MD simulation of this material in a specific thermodynamic ensemble gives very reasonable results. Unfortunately, under ion irradiation, the thermodynamic equilibrium condition does not hold. In the process of momentum and energy transfer, the colliding atoms can approach each other much closer and the potential, which was fitted to reproduce the thermodynamically equilibrated parameters, has no information about the nature of interactions at these short distances. The best solution that can be used to circumvent this problem is to spline the interatomic potential and the ZBL potential to introduce strong repulsive interactions within MD.

The other feature of MD method, which also requires special attention is the time step, which is used in the MD iteration loop. Usually it is selected to be rather short that the atom cannot advance too far during a single MD step. In the equilibrium simulations, when the energies of atoms are varying only insignificantly, using a fixed time step is reasonable. However, in the cascade simulations, a single particle may have very high energy, which would allow it to move too far within a fixed time step, such that it would cause the non-conservation of energy and instability in MD calculations. If the time step is fixed to a very small value, then after the ballistic phase, the simulations will proceed very slowly, and the simulation time will be unreasonably long. This is why, the adaptive time step is necessary to advance the time depending on the highest value of the energy in the system Nordlund (1995).

3 Interatomic potentials for simulation of non-equilibrium effects

Both the BCA and MD simulations rely on interatomic potentials. The solution of the scattering integral in BCA relies on a repulsive interatomic potential

$$V_{highE,rep,ij}(r_{ij})$$

, and this part also dominates strong collisions (kinetic energy roughly > 10 eV) in MD. The procedures to obtain these are well established. Ziegler, Biersack and Littmark have from an averaging procedure formulated a simple analytical "universal repulsive potential" for all atom pairs Z_1-Z_2, that is typically valid to within $\sim 5\%$ in the high-energy region of interest (Ziegler et al 1985). An alternative universal analytical potential has more recently been developed by Zinoviev (A. N. Zinoviev 2015). Quantum chemical calculations specific to a given Z_1-Z_2 pair can be used to calculate repulsive potential accurate to within $\sim 1\%$ (Nordlund et al 1997) which is comparable to the accuracy of the best experiments (Zinoviev and Nordlund 2017).

A typical curve illustrating the ZBL potential is shown in Fig. **??**, which also illustrates one of the quantum chemical potentials that also have an attractive part (corresponding to the bound state of a dimer molecule).

The equilibrium potential required for MD simulations are far less accurately known. For simulations of ion irradiation, it is crucial to use equilibrium potentials where chemical bonds can break. Hence in this article, we only consider so called "reactive" potentials, i.e. potentials where all bonds between atoms can break and reform (contrary to the case of almost all molecular mechanics force fields (Leach 2001). In general, these can be written in the form

$$V_i = \sum_j V_{rep,ij}(r_{ij}) + \sum_{jk} V_{attr,ijk}(r_{ij}, r_{ik}, \Theta_{ijk}) \tag{3}$$

Here V_i denotes the energy of atom i, and j and k indices of neighboring atoms. Typically, the equilibrium potentials are constructed for near-equilibrium properties, and hence are not consistent with the high-energy repulsive part $V_{highE,rep,ij}(r_{ij})$. In MD simulations that involve also high-energy collision cascades, it is thus customary to join the $V_{highE,rep,ij}(r_{ij})$ and $V_{rep,ij}(r_{ij})$ smoothly e.g. with fifth-order spline interpolation function or by summation with a function that goes smoothly from 1 to 0 in a narrow distance interval (Nordlund et al 1996). Usually this joining is done just by finding a functional form that gives a smooth connection between the two parts. However, recently the effect of the joining on damage production has been examined systematically (Sand et al 2016), and sometimes it is carefully adjusted via DFT calculations (Belko et al 2002; Stoller et al 2016).

The swift heavy ion track formation induced by the electronic excitations leads to kinetic energies of atoms of the order of 10 eV (although as evident from the discussion above, the exact mechanism of energy transfer to the atoms remains unclear, the observations of destruction of even strong covalent crystals implies that at least some atoms do get energies clearly above the cohesive energies, that are of the order of 5 eV). Hence for swift heavy ion effects above the synergy regime, it is in principle sufficient to have a good equilibrium potential. In the remainder of this section, we discuss briefly some of the classes of interatomic potentials that have been used in collision cascade and track simulations, as a comprehensive review of the vast field of interatomic potential development is beyond the aims of this article. Metals can be well described with so called embedded-atom method (EAM) potentials (Daw et al 1993). These can, via effective-medium theory, be motivated from fully quantum mechanical density functional theory (Puska et al 1981; Manninen

1986). Originally (Foiles et al 1986), they were formulated in the form

$$V_i = \sum_j V_{rep,ij}(r_{ij}) + F_i(\sum_j \rho_j(r_{ij})) \tag{4}$$

Here ρ_j is the electron density from atom j, and F_i is the energy that the solid gains when the ion core (metal atom without free electrons) is embedded in this electron density. Originally the EAM potentials were constructed with ?real? electron densities, however most recent implementations use ρ_j as fitting function of arbitrary form. In many potentials, the functional form of F_i is simply the square root function, which can be well motivated from the second-moment approximation of tight-binding electron structure models (Finnis and Sinclair 1984; Brenner 1989; Cleri and Rosato 1993; Albe et al 2002). Regardless of exact physical motivations, all potentials that share the basic functional form 3 can be called *EAM-like potentials*.

Regarding ionic materials, it is natural to seek a description of them based on the Coulomb potential between two different atomic charges q_i and q_j. These give directly the V_{attr} attractive part as pair potentials, while the repulsive part V_{rep} can e.g. be a simple exponential, similar to the EAM-like potentials. For highly ionic materials near equilibrium, such a simple pair potential description is well motivated physically. However, one has to bear in mind that under irradiation, atoms can come far away from their initial positions, and e.g. can start forming N gas bubbles in some nitrides (Kucheyev et al 2001). For describing such processes, fixed-charge ionic potentials are completely inappropriate, as they predict that the N-N interaction is completely repulsive. To circumvent this, one can (at least in principle) use charge-transfer interatomic potentials, where the charge of atoms depends on the local neighbourhood e.g. via electronegativity descriptions (Alavi et al 1992; Albe et al 2009; Yu et al 2007).

In materials where the bonding is a mixture of ionic and covalent bonding, a pure pair potential is not likely to give a good description of the material. A prototypical example of this is SiO_2, which while having a fairly high degree of ionicity, has a complex low-symmetry crystal structure with tetrahedrally arranged O atoms around the Si atoms. Such a structure cannot be described with pure pair potentials. Instead, a combination of an angular three-body term and an ionic one has proven to be suitable for describing at least the basic tetrahedral four-fold bonding of the Si atoms (Feuston and Garofalini 1988).

Materials with predominantly covalent bonding such as C, Si, Ge, and organic structures like hydrocarbons have a strong directional character of the bonds, due to the quantum mechanical hybridization of the valence electrons into sp^2 and sp^3 configurations. This hybridization leads to a preferred angle between bonds (120° for sp^2 and about 109.47° for sp^3), and hence it is natural to formulate potentials that give depend on the angle between bonds Θ_{ijk} and give an energy minimum at the preferred angle.

One widely used potential that utilises this approach is the Stillinger-Weber potential originally made for Si (Stillinger and Weber 1985). It has in principle the form

$$V_i = \sum_j V_{2,rep,ij}(r_{ij}) + \sum_{jk} V_{3,ijk}(r_{ij}, r_{ik}, \Theta_{ijk}) \tag{5}$$

i.e. has separate 2- and 3-body terms, where the 2-body term has both repulsive and attractive parts, and the three-body term has an explicit minimum at $\Theta_{ijk} = 109.47°$. Although relatively simple in form and formulated more than 30 years ago, it is still widely used and been found to describe fairly well properties far removed from its initial fitting database (Balamane et al 1992; Sastry and Angell 2003; Holmström et al 2010). It has also been extended for a wide range of other materials (Wang and Stroud 1988; Pailthorpe and Mahon 1990; Oligschleger et al 1996; Ichimura 1996; Aichoune et al 2000), including giving a non-ionic but rather successful description of SiO2 (Ohta and Hamaguchi 2001; Watanabe et al 2004; Samela et al 2008; Kluth et al 2008). While rather successful for Si, Ge and tetrahedral compound semiconductors, the Stillinger-Weber potential clearly is not suitable for carbon, which has the peculiar feature that the sp^2 (the bonding type in graphite and graphene) and sp^3 (diamond) bonding environments are almost identical in energy, i.e. two different bonding angles should have almost equal energy. To be able to describe several different bonding environments, Abell and Tersoff (Abell 1985; Tersoff 1988) developed a formalism based on Linus Paulings theory of the chemical bond (L. Pauling 1939). This formalism takes into account the observation by Pauling that the energy/bond decreases with increasing coordination number, and allows having local energy minima at several different bonding configurations – including the possibility to have the exact same energy for two of them. The potential is written to formally appear like a pair potential,

$$V_i = \sum_j V_{rep,ij}(r_{ij}) + \sum_j g_{ijk} V_{attr,ij}(r_{ij}). \tag{6}$$

However, the g_{ijk} term is constructed to also depend on the angle between bonds Θ_{ijk} and the coordination number of atom i . In effect, g_{ijk} modulates the strength of the attractive part in a manner consistent with the Pauling theory. This "Tersoff-like" general form, sometimes with slight variations in the functional form of the 3-body term g_{ijk}, has been parameterized for a very wide range of materials (e.g. (Ashu et al 1995; de Brito Mota and. J. F. Justo and Fazzo 1998; Matsunaga et al 2000; Humbird and Graves 2004; Juslin et al 2005; Billeter et al 2007; Powell et al 2007; Munetoh et al 2007), and interestingly has been shown to be with certain parameter choices consistent with the Finnis-Sinclair and tight-binding-motivated EAM-like potentials (Brenner 1989; Albe et al 2002).

The Tersoff formalism has also been extended for hydrocarbons [Bre90,Bre02], giving an interatomic potential that is fully reactive and can describe a wide range of carbon allotropes and hydrocarbon molecules. These potentials, variably called Brenner, REBO or AIREBO potentials, have been later implemented to include long-range forces (Stuart et al 2000) and also include oxygen, to enable simulation of carbohydrates (Ni et al 2004). They have been used to model several different kinds of irradiation effects, such as plasma-wall interactions (Salonen et al 2001; Träskelin et al 2004; Marian et al 2007) and low-energy recoil damage in

polyethylene and cellulose (Polvi et al 2012). The Brenner carbon potential, without the complex bond-conjugation terms, has also been found to be reasonably good in describing radiation effects in carbon nanotubes and graphene (for a review of the extensive works in this area, see (Krasheninnikov and Nordlund 2010)).

Studying swift heavy ion effects in organic materials is challenging, in part because it is likely that much of the damage is produced by electronic effects causing bond breaking, in part because the atomic potentials for organic materials (like the Brenner one) are rather slow. However, in many cases organic materials can be described also well by so called coarse-grained models, in which the basic object is not single atoms, but parts of, or a full molecule. The simplest variety of such models is describing compact molecules as spheres interacting with a Lennard-Jones potentials. Such models have been used to get good insights into e.g. laser ablation (Zhigilei et al 1998; Schäfer et al 2002) and swift heavy ion irradiation of organic materials (Bringa et al 2002; Bringa 2003).

4 MD simulation of interaction of energetic ions with materials

As mentioned earlier, incident ions interact with irradiated materials in two distinct ways, either via direct collisions with atoms of the material or via excitation of electronic subsystem, which are described by nuclear, S_n and electronic, S_e, stopping powers, respectively. Typical S_n and S_e curves are shown in figure 2. As one can see, both regimes are well separated to large extent, however, the energy regions were both nuclear and electronic stopping powers are significant also exist. Atomic collisions in the regime of nuclear stopping power can be simulated directly, the interaction of ions with electronic subsystem in the electronic stopping power regime ($>$ 100 keV/amu) requires development of additional multiscale models to enable these effects within a classical MD. With exception of a few key details which need to be paid thorough attention in the simulations of energetic atomic cascades in MD, in this chapter we will mostly focus on the electronic effects in materials, as this is a new area of application of atomistic simulations, where the methodology is still under development.

4.1 Collision cascades: nuclear stopping power

Unlike the BCA approach, the MD simulation cell must be constructed according to the crystal or amorphous structure of the material and thoroughly equilibrated in the suitable potential that all atoms assume the sites, which correspond to the lattice site in the chosen thermodynamic ensemble. The size of the cell must be sufficiently large to ensure that core of the cascade is in the middle of the cell and sufficiently far from the borders of the simulation cell. Introducing an energetic particle into the cell can be done either from the outside of the cell (simulation the near-surface radiation

effects) or by randomly selecting an atom of the cell and giving it a recoil energy in a random direction. The latter approach will emulate the evolution of a cascade inside the bulk. Bearing in mind a small size of the MD simulation box (a couple of hundred nanometers at most), these simulations can be thought as representative of a small box cut out from the real, very large bulk system.

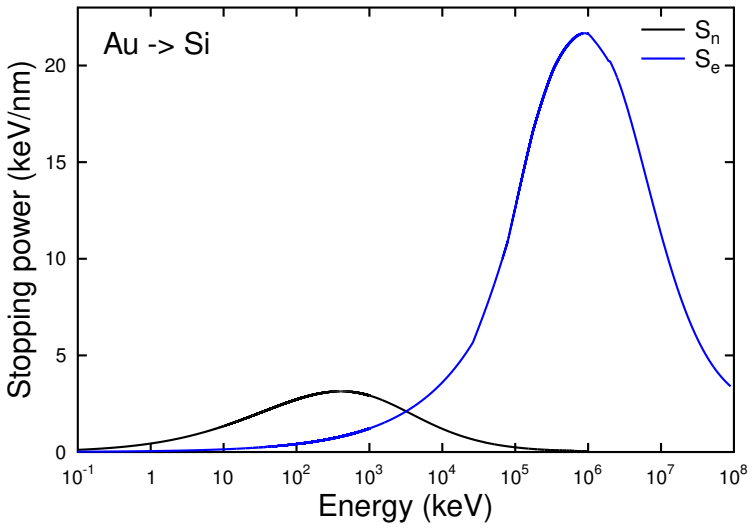

Fig. 2 Nuclear (S_n) and electronic (S_e) stopping powers in Si as a function of Au ion energy as calculated by TRIM95 software. (Ziegler 1995)

4.2 Electronic stopping power

Electronic effects are not explicitly taken into account within the classical molecular dynamics simulations. Solving the time-dependent (TD) Schrdinger equations for the atomic system with a highly energetic particle moving through became possible recently (most commonly using a TD-DFT approach) (Pruneda et al 2007; Correa et al 2012; Zeb et al 2012; Ojanperä et al 2014). Hence solving time-dependent Schrdinger's equation at every step between the collisions, as well as during the collision by MD, may provide an accurate answer on energy loss to the excitations in electronic subsystem, however, to date this approach is computationally very expensive.

Instead, simplified approximations can be used to take into account the energy loss due to electronic stopping power, which agree fairly well with experiments. Following the basic idea of BCA simulations, the electronic stopping power can be

implemented also in MD as a so-called frictional force. The implementation of the friction force in MD is similar to the algorithm used in SRIM, namely, the moving atom loses the energy between the collisions proportional to its velocity. The function $-(\frac{dE}{dx})_e(v)$ is obtained e.g. from the broad SRIM database, where the experimental measurements for different materials as well as theoretical estimations, if such measurements are not available, are collected (Ziegler ????). This has been implemented in MD by several groups (Pronnecke et al 1991; Nordlund 1995; Nordlund et al 1998; Cai et al 1998; Hou et al 2000; Duffy and Rutherford 2007; Duvenbeck et al 2007; Sandoval and Urbassek 2009), and demonstrated to work well by comparisons of experimental and simulated ion range distributions (Sillanpää et al 2001; Peltola et al 2006).

This approach, however, does not allow taking into account the energy, which may be returned back to the lattice atoms via electron-phonon coupling mechanism (Flynn and Averback 1988; Koponen 1992). The first attempt to introduce an analytical expression for calculation of cooling of the heat released in a cascade in metals by electrons was made in (Finnis et al 1991). This approach was developed later by M. Hou (Hou et al 2000), deriving the parameters for the electron-phonon coupling from the Sommerfeld model, giving a simple way to include the electron-phonon coupling on atoms as a frictional force. These approaches can give insight into the role of electron-phonon coupling on collision cascade development in the nuclear stopping regime (Pronnecke et al 1991; Björkas and Nordlund 2009). However, they are not suitable for modelling swift heavy ions, where it is crucial to know how heat is transferred from an evolving hot electron system to atoms. For this purpose, models have been developed where the electronic heat conduction is modelled concurrently with the atomic dynamics by solving the heat conduction equations as a function of space, and coupling the electronic and atomic heat locally (Duffy and Rutherford 2007; Vazquez et al 2017).

4.3 Thermostats for simulations of radiation effects in materials

Nuclear and electronic stopping powers imply that the incident energy is deposited to the irradiated material partly as potential (multiple defects remaining in the structure after the irradiation) and partly as kinetic energy. While the former form of the deposited energy is of interest as a result of the simulation, the latter may result in artificial heating of the lattice. The heating of irradiated samples is also observed in experiments if the irradiation fluxes are high and the sample is not well coupled to the surrounding, and special care is taken to keep the irradiated sample under the same temperature condition. Analogously, in molecular dynamics simulations of collision cascades or swift heavy ions, it is important to ensure that the extra heat is removed from the finite simulation cell, not to introduce an artificial heating of the system.

The standard approach to achieve this is to remove heat from the system at the boundaries, far from the high-energy recoils or ion track. This can be done in sev-

eral different ways: by linear scaling (Nordlund et al 1994) of velocities or using the Langevin (Caturla et al 1996) or Berendsen (Nordlund et al 1998) thermostats. Although none of these approaches can perfectly damp the pressure wave emanating from cascades, system size and parametric scaling studies can be easily used to determine whether the actual damage production results are affected by the boundary scaling (Samela et al 2005).

5 Modelling radiation damage produced by swift heavy ions

In the the electronic stopping power dominated swift heavy ion (energy $>>$ 10 keV/amu) regime, the probability of individual collisions with atoms is rather negligible. Instead, the intense electronic excitation produces a narrow trail of permanent damage along the ion path – the ion track (R. L. Fleischer and Walker 1975). The complex nature of electronic stopping power is discussed in detail in several publications (Itoh and Stoneham 1998,?; Duffy et al 2012; Schiwietz and Grande 2011; Rethfeld et al 2014), however, none of them suggests an accurate model free of fitting parameters, which can be directly implemented in atomistic simulations.

Different mechanisms of how electronic excitations may result in permanent damage in materials, which have been proposed thus far, are: (i) heating of a track core through electron-phonon coupling (a two-temperature model) (Toulemonde et al 2006; Duffy et al 2012); (ii) Coulomb explosion, which may be caused by many electrons being rapidly excited out of the core because of the passing ion (Bringa 2003); (iii) "cold melting", i.e. electrons being excited into antibonding states causing bond breaking (Gorbunov et al 2014; Medvedev et al 2015a,b); and finally, (iv) plasma formation in the track core (Cherednikov et al 2013a,b). All models are dramatically different, in that the model (i) explains everything by rapid heating of the track core into temperatures of the order of 100 000 K, while model (iii) states that the material can be damaged even if the temperature never exceeds the melting point of about 2 000 K. The models (ii) and (iv) are more specific to certain materials, where the charge relaxation may delay by a few ps.

Historically, the Coulomb explosion mechanism was the first mechanism, which was suggested to explain formation of nuclear particle tracks in minerals to analyze the records of energetic radiation in lunar rocks (Fleischer et al 1965; R. L. Fleischer and Hubbard 1967). Already then, the authors admitted that this model describes best the track formation in polymers, which was clearly confirmed later by Schiwietz et al. in (G.Schiwietz et al 2004). Bringa et al. (Bringa and Johnson 2002) showed that Coulomb explosion on the early stage in combination with thermal spike on a later stage are able jointly explain high electronic sputtering yields in polymeric materials. In other materials, the Coulomb explosion mechanism has not been confirmed, however, we mention here the attempt to explain track formation in Pd_80Si_20 metallic glass, where the authors observe plastic flow in the wake of the projectile, which may have been caused by Coulomb explosion inducing metal polarization (Klaumünzer et al 1986). However, it is generally accepted that in many

solid materials the charge neutralization time is too short to cause any significant displacement of atoms (Duffy et al 2012).

The model (iii), known mostly as "cold melting" or also as "lattice destabilization" assumes the modification of interatomic interactions due to electronic excitations. The equilibrium state of bonds in non-excited system will be different from that in the system, where the atoms forming the bonds are excited. If the excitation lasts sufficiently long time, it may cause strong displacements in vicinity of the excitation, leading to fast melting (at temperatures much below the melting point) known as athermal (or sometimes also non-thermal) melting. Although very interesting, this mechanism has inherent problem of implementation in atomistic simulations as it requires a modification of interatomic potential depending on the excited state of the atoms. Some attempts to take this process into account were performed by Rymzhanov et al. in (Rymzhanov et al 2016) using density functional theory calculations, however, the validity of such an approach is not fully justified.

Finally, there are also several attempts to explain the formation of ion tracks by using so called thermal spike model. This model was proposed to quantify track formation mostly in insulators as it implies thermal heat exchange between electronic and atomic subsystems. Strictly speaking, a thermal spike does not explain how the energy was deposited to electrons, but rather describes the system after an electronic temperature has reached locally a thermal equilibrium. The thermal spike could result from an initial Coulomb explosion (Bringa and Johnson 2002) or changes in the interatomic forces (Itoh et al 2009). The thermal energy of electrons is transferred then to the atoms via electron-phonon coupling, heating the lattice to the temperatures, which may cause atomic disorder (e.g. melting or boiling). Knowing the electronic stopping power and assuming a Gaussian distribution of the energy deposition around the track core, and that the temperature within the track must rise, at least, to the melting point, it was possible to deduce the radius of the disordered track (G.Szenes 2005). Toulemonde et al. proposed to deduce the melt radius by solving analytically a coupled system of heat equations written separately for electronic (T_e) and ionic (T_i) temperatures (Toulemonde et al 2000a):

$$\begin{cases} C_e \frac{\delta T_e}{\delta t} = \nabla(K_e \nabla T_e) - G(T_e - T_i) + B(r,t) \\ \rho C_i(T_i) \frac{\delta T_e}{\delta t} = \nabla(K_i(T_i) \nabla T_i) + G(T_e - T_i) \end{cases} \tag{7}$$

Here, $T_{e,i}$,$C_{e,i}$, $K_{e,i}$ are local temperature, specific heat capacity and heat conduction of electronic and ionic subsystems and G is the electron-phonon coupling parameter. The function $B(r,t)$ describes the energy density supplied to electronic system during the SHI path. Integrating this function over the time and space must result in the measured value of $\frac{dE}{dx}_e$. This model is mainly known as the inelastic thermal spike (i-TS) model (to distinguish it from a thermal spike developed in dense collision cascades). Since the model follows the evolution of two temperatures T_e and T_i, the model is also called the two-temperature model. This two-temperature approach is based on the model, which was developed by Kaganov (Kaganov et al 1957) and Lifshits (Lifshits et al 1960) for metals and then, it was applied to study laser (Fujimoto et al 1984) and SHI induced effects also in metals (Wang et al 1994).

Application of this model to insulators is not rigorously proven, however, using fitting parameters in the two-temperature equations, good agreement with experiments was shown also for different insulators (Toulemonde et al 2006).

6 Modelling of SHI impacts by using MD methods

Since electronic stucture is not explicitly described in MD algorithm, it is not immediately clear and straightforward how a SHI impact can be modelled by using this method. One of the first attempt to simulate the SHI impact in MD was made by Urbassek et al. (Urbassek et al 1994). In these simulations, a cylindrical track of a given radius was instantaneously energized by giving a constant energy, E_0, to all atoms within this track. Similar approach was used also in later papers by Bringa et al. (Bringa and Johnson ????, 2002). In the latter works, these and other authors used the value of the stopping power $\frac{dE}{dx}_e$ integrated over the length of the simulation cell to estimate the amount of energy, which can be given to the atoms in the track to simulate more realistic impacts (N. W. Lima and Papaléo 2016; Lan et al 2013; Jiang et al 2013; Lang et al 2015; A. Rivera and J. Olivares and A. Prada and M. L. Crespillo and M. J. Caturla and E. M. Bringa and J. M. Perlado and O. Pena-Rodriquez 2017). The profile in these simulations can be either flat or distributed as Gaussian with the standard deviation about 1-2 nm. Although rather primitive, this model of instantaneous energy deposition can already provide valuable insights on how the lattice can accommodate the energy in a restricted volume and what is the structure of the tracks inside. For instance, it was shown that track formation in different oxides is driven by competition of heat and mass transfer, fast quenching of the molten phase and eventual recrystallization. However, what remains unclear is the size of the restricted region where this energy has to be deposited. Usually the radius of the track is left as the free parameter and the simulations are made for a number of combinations of E_0 and r_{tr} with results compared to the experiment (Urbassek et al 1994; Bringa and Johnson 2002).

It is also possible to benefit from existing *i*-TS model and develop a multiscale approach, where the equations 5 are solved numerically until the heat is maximally transferred from electronic to ionic subsystem at time t_{max} (usually around 100 fs) and then, translate the temperature profile $T_i(r,t_{max})$ into kinetic energies of atoms in the simulation cell (Kluth et al 2008; Pakarinen et al 2009; Leino et al 2015). Since the *i*-TS model uses the parameters of the system obtained in thermal equilibrium, it is necessary to adjust the profile $T_i(r,t_{max})$ scaling it to the melting point given by the potential in use. As it was shown, the choice of the model how the energy is deposited to the simulation cell may affect significantly the simulation results (Mookerjee et al 2008), where significant differences in the sputtering rates as predicted by the inelastic thermal spike deposition and the cylinder model was reported.

In all aforementioned methods, it is important to set correctly the boundary conditions. For instance, periodic boundary conditions can be used to mimic the bulk

case (all directions periodic) and the surface can be simulated by leaving one direction to be open (non-periodic). Despite the choice of the boundary, the limited size of the simulation cell (finite number of atoms) causes two simulation artefacts. First of all, a strong shock wave, which is generated in the cell after the energy was introduced in the center of the track only, will return back to the track passing through periodic boundary condition. Moreover, the heat that is introduced in the cylindrical center of the cell, eventually will spread in the cell and thermalize at the temperature, which is much higher than expected if heat conduction is assumed. Hence, a special attention must be paid to mimic heat conduction effect to the bulk and to dampen the pressure waves from the track. To achieve this goal, the velocities of the atoms near the boundaries of the simulation cell must be scaled by using, e.g. Berendsen thermostat. A more advanced method to cancel the pressure wave was introduced in Ref. (Zhigilei and Garrison 1999).

6.1 Two-temperature molecular dynamics model

The two-temperature MD (2TMD) model follows the temperature evolution in electronic and ionic subsystems directly within MD simulations. It can be done by using a Langevin thermostat with the friction force added to the MD equations of motion of atoms:

$$m_i \mathbf{a}_i = \mathbf{F}_i(t) + \xi m_i \mathbf{v}_i \tag{8}$$

Here, m_i, $\mathbf{a}_i$, $\mathbf{F}_i$ and $\mathbf{v}_i$ are mass, acceleration, force and velocity of a given atom i. The value ξ is estimated as

$$\xi = \frac{VG(T_r)(T_e - T_i}{\Sigma_i m_i v_i^2} \tag{9}$$

In this model, the simulation cell is divided into smaller cells of equal volume V, where electronic and ionic temperatures are averaged separately, see figure 3. Within this geometry, the boundary condition can be set to the desired temperature to imitate the heat conduction to the bulk. Moreover, the size of the ionic and electronic structure does not need to be the same. By imposing a larger mesh for electronic subsystem, the electronic temperature can be converged to the desired bulk temperature in more gradual manner. This model was initially used to simulate the short-pulse laser melting (Ivanov and Zhigilei 2003), but later on in was extended to be used to simulate the electronic effects in radiation damage simulations (Duffy and Rutherford 2007).

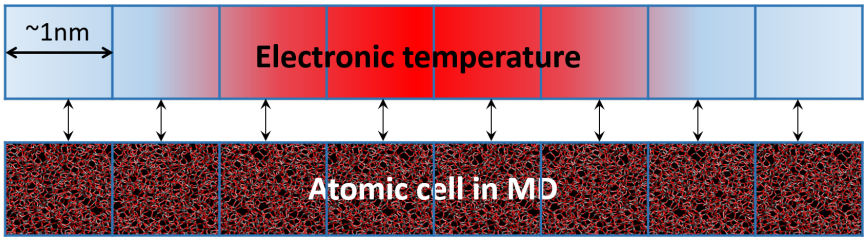

Fig. 3 Illustration of the 2TMD simulation cell. For clarity the grids of electronic and ionic subsystem are shown separately. In each cell of the grid a local electronic and ionic temperature is defined. Dirichlet boundary condition is applied at the sides of the electronic temperature grid (light blue color). Size of the grid point should be sufficiently large to enable statistically meaningful values of local temperature.

6.2 Parameterization of the inelastic thermal spike model

Advantage of one implementation of the inelastic thermal spike model over the other, such as an instantaneously deposited energy or by a natural evolution within the 2TMD model, depends on the specific problem and the studied material. However, both implementations rely heavily on the parameters used in the model.

First of all, what remains ambiguous, is how the energy is deposited to the electrons by a SHI. In the original model by Toulemonde et al., the initial distribution of energy is described by the expression suggested by Waligorski et al. (Waligórski et al 1986). This distribution is then scaled to give stopping power predicted by the SRIM software (Ziegler ????).

There are more theoretical attempts to reproduce initial electronic cascades, especially in the short-pulse laser irradiation community (Rethfeld 2004), later on adopted for simulations of electronic effects during a SHI impact on materials by using Monte Carlo approach (Medvedev et al 2010, 2015a,b). These types of simulations may provide a more realistic distribution of initial energy deposition, giving deeper insight on the energy distribution taken away from the track by fast δ-electrons.

Furthermore, it is neither clear how to estimate parameters of electronic subsystem in such a far-from-equilibrium condition. Originally, in the Toulemonde's model (Toulemonde et al 2000b) the free electron gas model is used to estimate the electronic heat capacity ($C_e = \frac{3}{2} N_e k_B$, where N_e is the electron density and $k_B b$ is the Boltzmann constant) and conductivity ($K_e = D_e C_e = (\frac{1}{3} l v_f C_e)$ with D_e being the electron diffusivity, l and v_f the electron mean free path and Fermi velocity, respectively.) The electron-phonon coupling constant remained in the Toulemonde's model as a free parameter adjusted to result in the track radius observed in experiments.

The free-electron gas model leads to severe underestimation of the C_e parameter, since the electronic temperature may rise during the SHI impact by several orders of magnitude. In the limit when the electronic temperature homogenized, but still

$T_e >> T_i$, the equations 5 can be simply re-written as

$$C_e \frac{\delta T_e}{\delta t} = G \cdot (T_e - T_i) \tag{10}$$

Solving this equation gives a clear relationship between G and C_e:

$$\tau = \frac{C_e}{G} \tag{11}$$

where τ is the relaxation time, which can be obtained from pump-probe experiments by direct measurement of the electron temperature after laser pulse using angle-resolved photoemission spectroscopy(Johannsen et al 2013).

Daraszewicz et al. (Daraszewicz et al 2014) suggested the recipe to calculate the electron-phonon coupling from the first principles for W. However, this is less straightforward, if the studied material is an insulator. In this case, the specific heat capacity still can be calculated from $C_e = \frac{\delta E}{\delta T_e}$, where modification of the internal energy E is found from the analysis of the electronic density of states (DOS) obtained in finite-temperature generalisation of the density functional theory (DFT) using Quantum Espresso (Giannozzi et al 2009). If the value of the relaxation time is known experimentally, the strength of electron-phonon coupling can be estimated from equation 6.2. Figure 4 shows the difference between the electronic specific heat capacity calculated by using Quantum Espresso and the free-electron gas model (temperature-independent), where it is clear that C_e at low temperature is strongly overestimated, while at high electronic temperature it must be multifold higher.

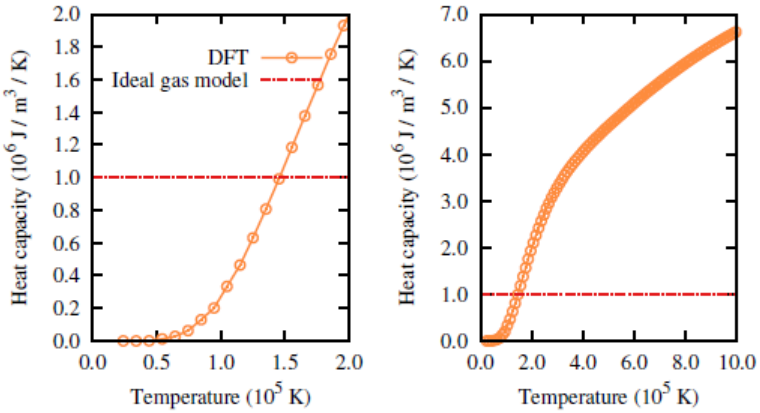

Fig. 4 Right: electronic temperature dependence of the specific-heat capacity $C_e(T_e)$ as calculated with DFT. The dash-dotted line shows the commonly used Ce from the free-electron gas model assuming two excited electrons (Toulemonde et al 2000b). Left: the same data at lower temperatures for clarity (Leino et al 2015)

7 Simulations of track formation in bulk materials

As described in section 5, simulation methods, which exist to date to simulate SHI impacts on materials, are still under development. However, already initial attempts to simulate this complex phenomenon with the available tools have resulted in a few very valuable insights, and we review here briefly a few significant examples.

The first experimental measurements of tracks in amorphous materials, e.g. a-SiO_2, by using small-angle X-ray scattering spectroscopy (SAXS) indicated the existence of a core-shell structure. By then, it was clear that the nature of ion track damage ranges from small differences between track and the rest of material in amorphous structures (e.g., SiO_2 (Klaumünzer 2004)), formation of point defect and defect clusters in ionic crystals (Trautmann et al 2000; Khalfaoui et al 2005) to amorphization of crystalline materials (e.g., InP (Kamarou et al 2008; Klaumünzer 2004; Meftah et al 1994a)). However, the new finding clearly showed that the subtle difference in densities appear even within a track region itself. Although it was clear that in the core of the track the density was different from that of a periphery, it was not obvious whether the ratio was towards the overdense shell and underdense core or the other way around. The insight on the track formation was possible through MD simulations. A few profiles obtained for different energy depositions with profiles calculated by using Toulemonde's *i*-TS model 5 are shown in comparison to the experimental profile reconstructed from the SAXS signals. It is clear that the ion track leaves a clear signature of an underdense core surrounded by the overdense shell, see figure 5.

The mechanism revealed in these simulations can be summarized as shown in figure 6. The energy deposited to the electronic subsystem in a SHI impact is subsequently transferred to the lattice via the electron-phonon coupling. Large amount of energy deposited nearly instantaneously (within a few hundreds of femtoseconds) in a limited volume of an ion track, leads to very fast phase transition within the track to a high-pressure vapour phase of the material, generating strong pressure waves, which transport the material from the track center. The cold material surrounding the track resist the wave propagation pressing the material to a higher density state. At the same time, the efficient heat exchange between the small volume of a heated track and cold, but infinitely large, surrounding bulk material dissipates the heat from the track freezing in the inhomogeneous density distribution around the track. Since a-SiO_2 is known to be highly viscous, the density variation remains as a permanent track after the impact region cooled down to the room temperature.

The combination of the *i*-TS model by Toulemonde (eqs. 5) and MD simulations would lead to a monotonic increase of the track radius approximately as the square root function of the deposited energy, which can be intuitively expected. However, this was not confirmed in the experiments (Afra et al 2013), where it was found that that the track radius saturates and does not exceed a certain value for the given material. Intriguingly, in the other experiments for the same material, a-SiO_2, the saturation of the track radius with increase of the stopping power was not observed while using a different technique, the Rutherford backscattering (RBS) (Meftah et al 1994a). Having in mind that specific heat capacity $C_e = \frac{\delta E}{\delta T_e}$ depends on the electron

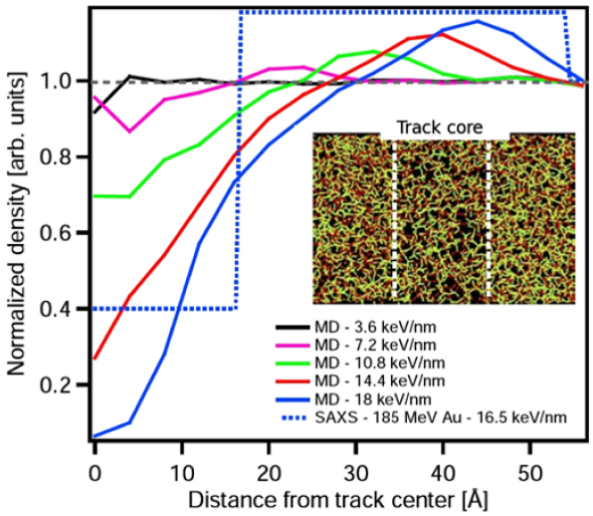

Fig. 5 Radial density profiles obtained in MD simulations for a-SiO_2 shown in arbitrary units. Unmodified density of the cell is shown with a dashed line at 1.0. The dotted line shows for comparison a density profile extracted from the SAXS measurements of the 185 MeV Au (Kluth et al 2008). The inset shows a snapshot of MD simulations at the moment when the track has already cooled down to its final state. The figure is reproduced from (Pakarinen et al 2010)

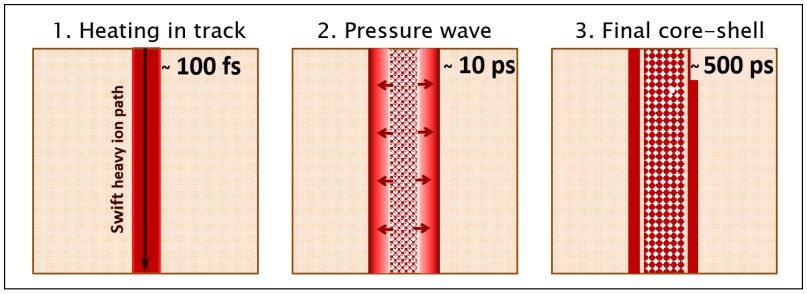

Fig. 6 Mechanism of track formation in amorphous materials. The track is heated in the narrow region around the swift heavy ion path. In the following few picoseconds, the pressure waves formed due to extremely high temperature gradient transport the material from the track core to the periphery of the track. The intense heat exchange with the infinite thermal bath of a surrounding material leads to the temperature quench and the structure freezes in the density-alternating state.

density of states, which are different at different electronic temperatures, one can calculate $C_e(T_e)$ as shown in figure 4. Plugging in this function to the full 2TMD model, the results show that indeed, the track radius saturates with increase of the stopping power. This is explained by rapid growth of the C_e at high electronic temperatures and thus the slower rise of the temperature in the track. Now, if we turn our sight to the defects, which are created out of the track radius, we see that the distance from the track center to the individual defects keeps increasing with increase

of the stopping power, although the track radius has already been saturated. Since the higher stopping power would produce higher energy δ-electrons, the individual defects formed in the electronic cascades initiated by the δ-electrons may locate further away from the track. This can explain the discrepancy between the SAXS (Afra et al 2013) and RBS (Meftah et al 1994a) experiments, since the former technique is sensitive to change of densities in the track, but the latter measures the defects and disordered regions. In figure 7, the MD track radii measured by analysing the density variations and the furthest defects found in the MD cell away from the center of the track are compared to the SAXS and RBS results. Although the MD track radii obtained by measuring the furthest defects are still somewhat smaller than the RBS signal, the growing trend is clear when it is compared to the saturated trend of the track radii obtained by measuring the density variation in the track.

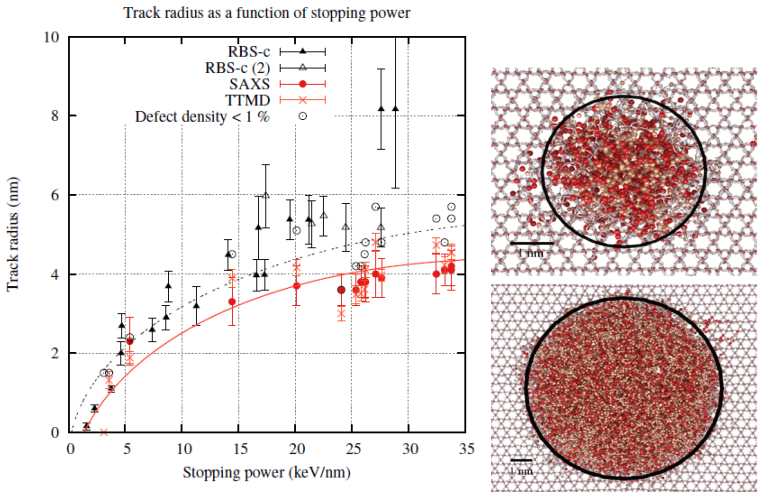

Fig. 7 a) Track radius as a function of stopping power. The experimental data are from refs. (Meftah et al 1994a; T.A.Tombrello 1984; Afra et al 2013). The lines are polynomial fits to the simulation data points to guide the eye. The empty circles indicate a radius at which the defect concentration falls below 1% in the simulations; b) Snapshots of tracks obtained with lower energy ions (27 MeV Au, top) and at the saturation region (1.4 GeV Au, bottom). The circles are the track radii that are obtained by fitting density variation. Defected atoms are drawn as large spheres.

Effect of the parameterization of equations 5 was also clearly observed in $SrTiO_3$ in (Weber et al 2014), where the reduction of the thermal conductivity of the electronic and ionic subsystems was associated with defects in a predamaged $SrTiO_3$ layer. By reducing these parameters by the order of magnitude, the authors found that track in the predamaged $SrTiO_3$ layer (with up to 1.5% of Frenkel pairs in the structure) was larger and compared much better to the tracks seen in the experiment. On the other hand, the SHI tracks were found to cause a healing effect in the pre-damaged SiC via the so-called SHIBIEC effect, which stands for swift heavy ion-induced epitaxial recrystallization (Debelle et al 2012, 2014). In these

experiments, the ideal zinc blende structure of 3C-SiC was predamaged by 100 keV Fe ions at room temperature with the fluences of $2 \times 10^{14} cm^2$ and $4 \times 10^{14} cm^2$ to achieve partial and full amorphization of a layer of the 3C-SiC sample. After introducing SHI tracks according to equations 5 generated by 0.87 GeV Pb ions, the damage existed in 3C-SiC partially recovered due to temperature induced recrystallization at the interface between crystal-amorphized phases of 3C-SiC. The lower degree of amorphization, the stronger recovery was achieved in both experiments and simulations, as shown in figure 8.

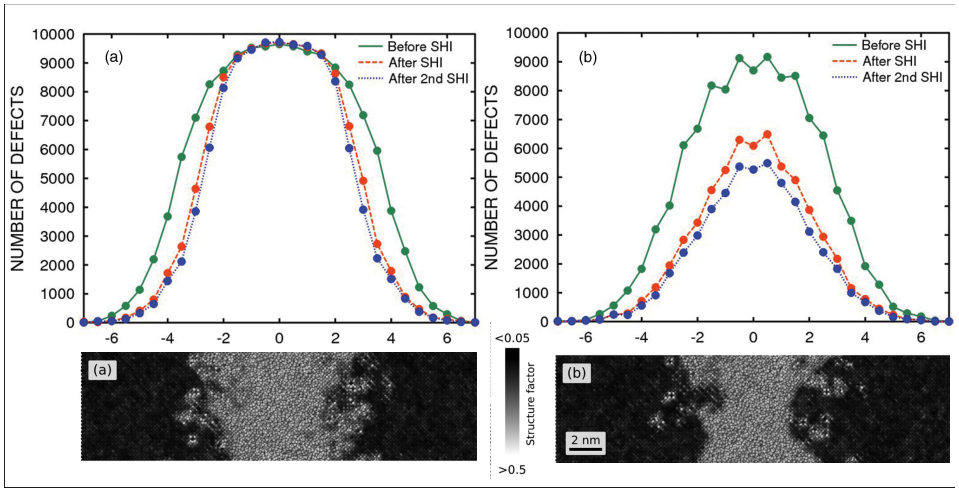

Fig. 8 Simulated depth distributions of the damage in the 3C-SiC cells damaged by low-energy recoils and subsequently heat treated by a thermal spike caused by 0.87 GeV Pb ions Case of (a) fully amorphous and (b) partially amorphous. The corresponding images of the analysis of angular structure factors show atomistic image of the recovered buried layer of the predamaged 3C-SiC.

One more interesting phenomenon, which was explained by using MD simulations of ion tracks was the formation of "bow-tie"-shaped voids in amorphous germanium. In this material, the heating induced by a SHI track has lead to a series of phase transitions within the track region (Ridgway et al 2013; Hooda et al 2017). Simulation of track evolution in amorphous germanium revealed the stages schematically illustrated in figure 9. First two stages are similar to track dynamics in other insulating materials: during the first 100 fs, the track core rapidly heats up, and the strong pressure waves transport the material away from the center of the track during the following 3 ps. While cooling down from a vapour to the liquid phase, a phase transition occurs: the hot low density liquid germanium turns into much denser cooler liquid germanium phase. This transition creates empty space and a multitude of small voids form along the track during another 10 ps. For more than 30 ps, the temperature in the track is sufficient to enable the coalescence of small voids into larger ones, which gradually contract along the track axis due to expansion of the amorphous Ge after a reverse phase transition from the liquid to

amorphous state, whose density is known to be lower. As a final shape of "bow-tie" shaped voids remain in the system at the times longer than 1 ns. The comparison of the simulated void in amorphous Ge and the TEM image of the void obtained with the same irradiation condition are shown in figure 10.

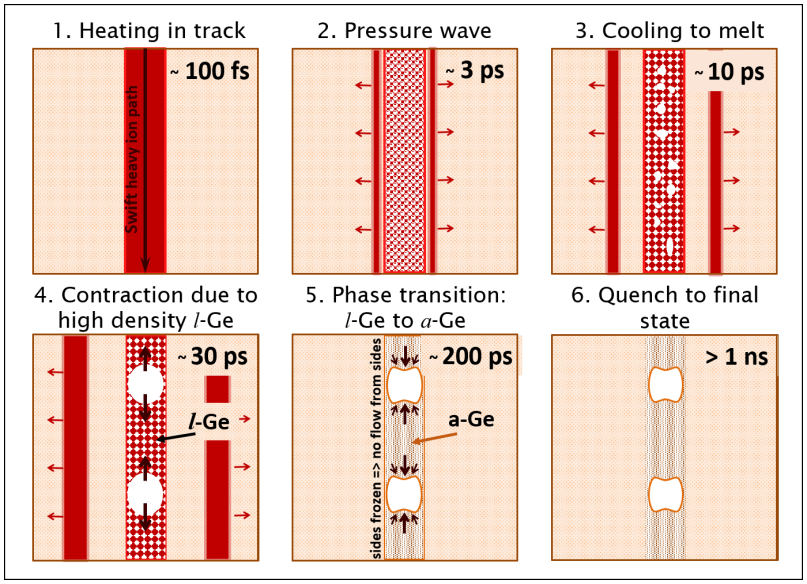

Fig. 9

8 Conclusions

In this Article, we have reviewed briefly the basic physics of materials modification by energetic ions or recoils, both in the nuclear and electronic damage regimes. We also discussed how molecular dynamics methods can be modified to model the ensuing damage, both in the nuclear and electronic collision regimes. Examples of recent results from especially the electronic damage regime are provided in the end.

Acknowledgements

References

A N Zinoviev (2015) Electron screening of the Coulomb potential at small internuclear distances.

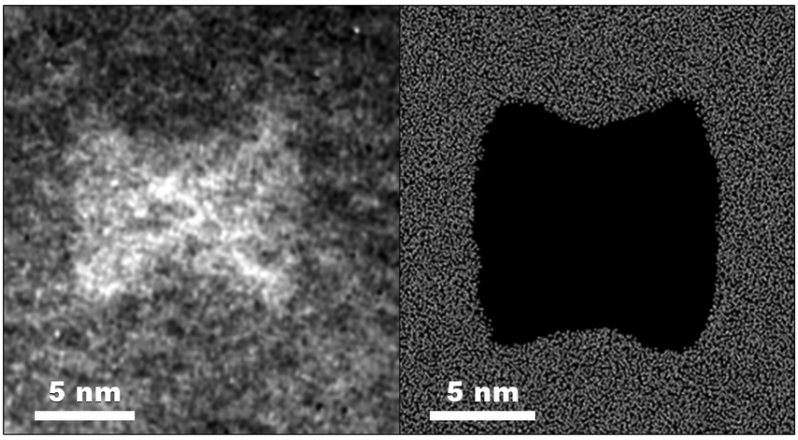

Fig. 10 On the left, a TEM image of a bowtie-shaped void formed in amorphous Ge by swift heavy ion irradiation. On the right, the void simulated by using *i*-TS model in combination with classical MD simulations during the same radiation conditions. The data used for the images is the same as in Ref. (Ridgway et al 2013)

Nuclear Instruments and Methods in Physics Research Section B: Beam Interactions with Materials and Atoms 354:308 – 312

A Rivera and J Olivares and A Prada and M L Crespillo and M J Caturla and E M Bringa and J M Perlado and O Pena-Rodriquez (2017) Permanent modifications in silica produced by ion-induced high electronic excitation: experiments and atomistic simulations. Sci Rep 7:10,641

Abell GC (1985) ?? Phys Rev B 31:6184

Afra B, Rodriguez MD, Trautmann C, Pakarinen OH, Djurabekova F, KNordlund, Bierschenk T, Giulian R, Ridgway MC, Rizza G, Kirby N, Toulemonde M, Kluth P (2013) Saxs investigations of the morphology of swift heavy ion tracks in α-quartz. Journal of Physics: Condensed matter 25:0455,006, also available at `stacks.iop.org/JPhysCM/25/045006`

Aichoune N, Potin V, Ruterana P, Hairie A, Nouet G, Paumier E (2000) An empirical potential for the calculation of the atomic structure of extended defects in wurtzite GaN. Comput Mater Sci 17:380

Alavi A, Alvarez LJ, Elliott R, MacDonald IR (1992) Charge-transfer molecular dynamics. Phil Mag B 65:489

Albe K, Nordlund K, Averback RS (2002) Modeling metal-semiconductor interaction: Analytical bond-order potential for platinum-carbon. Phys Rev B 65:195,124

Albe K, Nord J, Nordlund K (2009) Dynamic charge-transfer bond-order potential for gallium nitride. Phil Mag A 89:3477–3497

Allen MP, Tildesley DJ (1989) Computer Simulation of Liquids. Oxford University Press, Oxford, England

Apel P (2003) Swift ion effects in polymers: industrial applications. Nucl Instr Meth Phys Res B 208:11

Ashu PA, Jefferson JH, Cullis AG, Hagston WE, Whitehouse CR (1995) Molecular dynamics simulation of (100) InGaAs/GaAs strained-layer relaxation processes. J Cryst Growth 150:176–179

Averback RS, Diaz de la Rubia T (1998) Displacement damage in irradiated metals and semiconductors. In: Ehrenfest H, Spaepen F (eds) Solid State Physics, vol 51, Academic Press, New York, pp 281–402

Balamane H, Halicioglu T, Tiller WA (1992) Comparative study of silicon empirical interatomic potentials. Phys Rev B 46(4):2250

Belko V, Posselt M, Chagarov E (2002) Improvement of the repulsive part of the classical interatomic potential for SiC. Nucl Instr Meth Phys Res B 202:18–23

Bench MW, Robertson IM, Kirk MA, Jenčič I (2000) Production of amorphous zones in GaAs by the direct impact of energetic heavy ions. J Appl Phys 87(1):49–56

Billeter SR, Curioni A, Fischer D, Andreoni W (2007) Ab initio derived augmented Tersoff potential for silicon oxynitride compounds and their interfaces with silicon. Phys Rev B 73:155,329

Björkas C, Nordlund K (2009) Assessment of the relation between ion beam mixing, electron-phonon coupling, and damage production in Fe. Nucl Instr Meth Phys Res B 267:1830–1836

Brenner D (1989) ?? Phys Rev Lett 63:1022, shows that Tersoff and EAM formalisms are really the same in absence of angular terms

Bringa EM (2003) Molecular dynamics simulations of Coulomb explosion. Nucl Instr Meth Phys Res B 209:1–9

Bringa EM, Johnson RE (????) Coulomb Explosion Sputtering. ? Proceedings of Werner Brandt Workshop 1999

Bringa EM, Johnson RE (2002) Coulomb Explosion and Thermal Spikes. Phys Rev Lett 88(16):165,501

Bringa EM, Johnson RE, Papaleo RM (2002) Crater formation by single ions in the electronic stopping regime: Comparison of molecular dynamics simulations and experiments on organic films. Phys Rev B 65:094,113

Cai D, Snell CM, Beardmore KM, Grønbech-Jensen N (1998) Simulation of phosphorus implantation into silicon with a single parameter electronic stopping power model. International J Modern Physics C 9(3):459

Caturla MJ, T Diaz de la Rubia LAM, Gilmer GH (1996) Ion-beam processing of silicon at keV energies: A molecular-dynamics study. Phys Rev B 54(24):16,683

Chason E, Picraux ST, Poate M, Borland JO, Current MI, Diaz de la Rubia T, Eaglesham DJ, Holland OW, Law ME, Magee CW, Mayer JW, Melngailis J, Tasch AF (1997) Ion beams in silicon processing and characterization. J Appl Phys 81(10):6513–6561

Cherednikov Y, Sun S, Urbassek H (2013a) Hybrid paricle-in-cell/molecular dynamics simulation of swift heavy ion tracks in lif. Phys Rev B 87(24):245,424

Cherednikov Y, Sun S, Urbassek H (2013b) Sputtering from swift-ion trails in lif: A hybrid pic/md simulation. Nuclear Instruments and Methods in Physics Research B 315:313 – 317

Cleri F, Rosato V (1993) Tight-binding potentials for transition metals and alloys. Phys Rev B 48(1):22

Correa AA, Kohanoff J, Artacho E, Sanchez-Portal D, Caro A (2012) Nonadiabatic Forces in Ion-Solid Interactions: The Initial Stages of Radiation Damage. Physical Review Letters 108(21):213,201

Current MI, Wei CY, Seidman DN (1983) Direct observation of the primary state of damage of ion-irradiated tungsten II. Definitions, analyses and results. Phil Mag A 47(3):407

Daraszewicz S, Giret Y, Tanimura H, Duffy D, Shluger A, Tanimura K (2014) Determination of the electronphonon coupling constant in tungsten. Applied Physics Letters 105:023,112, URL http://scitation.aip.org/content/aip/journal/apl/105/2/10.1063/1.4890413

Daw MS, Foiles SM, Baskes MI (1993) The embedded-atom method: a review of theory and applications. Mat Sci Rep 9:251

Debelle A, Backman M, Thomé L, Weber WJ, Toulemonde M, Mylonas S, Boulle A, Pakarinen OH, Juslin N, Djurabekova F, Nordlund K, Garrido F (2012) Combined experimental and computational study of the recrystallization process induced by electronic interactions of swift heavy ions with silicon carbide crystals. Physical Review B 86:100,102(R), DOI 10.1103/PhysRevB.86.100102, also available at http://dx.doi.org/10.1103/PhysRevB.86.100102

Debelle A, Backman M, Thome L, Nordlund K, Djurabekova F, Weber WJ, Monnet I, Pakarinen OH, Garrido F, Paumier F (2014) Swift heavy ion induced recrystallization in cubic silicon carbide: new insights from designed experiments and md simulations. Nuclear Instruments

and Methods in Physics Research B 326:326 – 331, DOI 10.1016/j.nimb.2013.10.080, also available at http://dx.doi.org/10.1016/j.nimb.2013.10.080

Djurabekova F, Samela J, Timko H, Nordlund K, Calatroni S, Taborelli M, Wuensch W (2012) Crater formation by single ions, cluster ions and ion "showers" . Nucl Instr Meth Phys Res B 272:374–376, DOI http://dx.doi.org/10.1016/j.nimb.2011.01.104

Duffy DM, Rutherford AM (2007) Including the effects of electronic stopping and electron-ion interactions in radiation damage simulations. J Phys Cond Matter 19:016,207

Duffy DM, Daraszewicz S, Mulroue J (2012) Modelling the effects of electronic excitations in ionic-covalent materials. Nuclear Instruments and Methods in Physics Research B 277:21 –27

Duvenbeck A, Weingart O, Buss V, Wucher A (2007) Electron promotion and electronic friction in atomic collision cascades. New J Physics 9:38

Feuston BP, Garofalini SH (1988) Empirical three-body potential for vitreous silica. J Chem Phys 89(9):5818

Finnis MW, Sinclair JE (1984) A simple empirical N-body potential for transition metals. Phil Mag A 50(1):45, *see also Erratum, ibid. 53 (1986) 161*

Finnis MW, Agnew P, Foreman AJE (1991) Thermal excitation of electrons in energetic displacement cascades. Phys Rev B 44(2):44

Fleetwood D, Kosier S, Nowlin R, Schrimpf R, Reber R, Delaus M, Winokur P, Wei A, Combs W, Pease R (1994) Physical-mechanisms contributing to enhanced bipolar gain degradation at low-dose rates. IEEE Transactions on nuclear science 41(6):1871–1883, 1994 IEEE Annual Conference on Nuclear and Space Radiation Effects (NSREC 94), TUCSON, AZ, JUL 18-22, 1994

Fleischer R, Price P, Walker RM (1965) Ion explosion spike mechanism for formation of charged-particle tracks in solids. Journal of Applied Physics 36:3645

Flynn CP, Averback RS (1988) Electron-phonon interactions in energetic displacement cascades. Phys Rev B 38:7118

Foiles SM, Baskes MI, Daw MS (1986) Embedded-atom-method functions for the fcc metals Cu, Ag, Au, Ni, Pd, Pt, and their alloys. Phys Rev B 33(12):7983, *Erratum: ibid,* Phys. Rev. B 37, 10378 (1988)

Fujimoto JG, Liu JM, Ippen EP, Bloembergen N (1984) Femtosecond laser interaction with metallic tungsten and nonequilibrium electron and lattice temperatures. Phys RevLett 53:1837 – 1840

Gallagher K, Brown R, Johnson C (1998) Fission track analysis and its applications to geological problems. Annual Review of Earth and Planetary sciences 26:519–572

Giannozzi P, Baroni S, Bonini N, Calandra M, Car R, Cavazzoni C, Ceresoli D, Chiarotti GL, Cococcioni M, Dabo I, Corso AD, de Gironcoli S, Fabris S, Fratesi G, Gebauer R, Gerstmann U, Gougoussis C, Kokalj A, Lazzeri M, Martin-Samos L, Marzari N, Mauri F, Mazzarello R, Paolini S, Pasquarello A, Paulatto L, Sbraccia C, Scandolo S, Seitsonen GSAP, Smogunov A, Umari P, Wentzcovitch RM (2009) Quantum espresso: a modular and open-source software project for quantum simulations of materials. Phys: Condens Matter

Gorbunov SA, Medvedev NA, Rymzhanov R, Terekhind PN, Volkov AE (2014) Excitation and relaxation of olivine after swift heavy ion impact . Nucl Instr Meth Phys Res B 326:163 – 168

GSchiwietz, KCzerski, MRoth, FStaufenbiel, Grande P (2004) Femtosecond dynamics snapshots of the early ion-track evolution. Nuclear Instruments and Methods in Physics Research Section B 226(4):683 – 704

GSzenes (2005) Ion-induced amorphization in ceramic materials. J Nucl Mater 336(1):8 – 89

Holmström E, Krasheninnikov AV, Nordlund K (2010) Quantum and Classical Molecular Dynamics Studies of the Threshold Displacement Energy in Si Bulk and Nanowire. In: Ila D, Lindner JKN, Chu PK, Baglin J, Kishimoto N (eds) Ion Beams and Nano-Engineering, MRS Symposium Proceedings, vol 1181, MRS, Warrendale, PA, USA, pp 111–122

Hooda S, Avkhachev K, Khan S, Djurabekova F, K Nordlund K, Satpati B, Bernstorff S, Ahlawat S, Kanjilal D, Kabiraj D (2017) Mechanistic details of the formation and growth of nanoscale voids in Ge under extreme conditions within an ion track. J Phys D: Appl Phys 225302

Hou Q, Hou M, Bardotti L, Prevel B, Melinon P, Perez A (2000) Deposition of AuN clusters on Au(111) surfaces. I. Atomic-scale modeling. Phys Rev B 62(4):2825–2834

Humbird D, Graves DB (2004) Molecular dynamics simulations of Si-F surface chemistry with improved interatomic potentials. Plasma Sources, Science and Technology 13(3):548

Ichimura M (1996) Stillinger-Weber potentials for III-V compound semiconductors and their application to the critical thickness calculation for InAs/GaAs. Physica Status Solidi A 153(2):431–7

Itoh N, Stoneham A (1998) Excitonic model of track registration of energetic heavy ions in insulators. Nuclear Instruments and Methods in Physics Research B 146:362 – 366

Itoh N, Duffy D, Khakshouri S, Stoneham A (2009) Making tracks: electronic excitation roles in forming swift heavy ion tracks. J Phys: Condens Matter 21:474,205, DOI http://dx.doi.org/10.1088/0953-8984/21/47/474205

Ivanov DS, Zhigilei LV (2003) Combined atomistic-continuum modeling of short pulse laser melting and disintegration of metal films. Phys Rev B 68:064,114

de Brito Mota and J F Justo F, Fazzo A (1998) Structural properties of amorphous silicon nitride. Phys Rev B 58:8323

Jiang W, Devanathan R, Sundgren C, Ishimaru M, Sato K, Varga T, Manandhar S, Benyagoub A (2013) Ion tracks and microstructures in barium titanate irradiated with swift heavy ions: A combined experimental and computational study. Acta Materialia 61:7904 – 7916

Johannsen JC, Ulstrup S, Cilento F, Crepaldi A, Zacchigna M, Cacho C, Turcu ICE, Springate E, Fromm F, Raidel C, Seyller T, Parmigiani F, Grioni M, Hofmann P (2013) Direct view of hot carrier dynamics in graphene. Phys Rev Lett 111:027,403

Juslin N, Erhart P, Träskelin P, Nord J, Henriksson KOE, Nordlund K, Salonen E, Albe K (2005) Analytical interatomic potential for modelling non-equilibrium processes in the W-C-H system. J Appl Phys 98:123,520

Kaganov MI, Lifshitz IM, Tanatarov LV (1957) Relaxation between electrons and crystalline lattice. Sov Phys JETP 4(2):173

Kamarou A, Wesch W, Wendler E, Undisz A, Rettenmayr M (2008) Radiation damage formation in inp, insb, gaas, gap, ge, and si due to fast ions. Phys Rev B 78:054,111

Khalfaoui N, Rotaru CC, Bouffard S, Toulemonde M, Stoquert JP, Haas F, Trautmann C, Jensen J, Dunlop A (2005) Characterization of swift heavy ion tracks in caf2 by scanning force and transmission electron microscopy. Nucl Inst and Meth in Phys Res B 240(4):819 – 828, DOI https://doi.org/10.1016/j.nimb.2005.06.220

Klaumünzer S (2004) Ion tracks in quartz and vitreous silica. Nuclear Instruments and Methods in Physics Research B 225:136

Klaumünzer S, dong Hou M, Schumacher G (1986) Coulomb explosions in a metallic glass due to the passage of fast heavy ions? Phys Rev Lett

Kluth P, SchnohrCS, Pakarinen OH, Djurabekova F, Sprouster DJ, Giulian R, Ridgway MC, Byrne AP, Trautmann C, Cookson DJ, Nordlund K, Toulemonde M (2008) Fine structure in swift heavy ion tracks in amorphous SiO_2. Phys Rev Lett 101:175,503

Koponen I (1992) Atomic mixing in ion-bombardment-induced temperature spikes in metals. J Appl Phys 72(3):1194

Krasheninnikov AV, Nordlund K (2010) Ion and electron irradiation-induced effects in nanostructured materials. J Appl Phys (Applied Physics Reviews) 107:071,301

Kucheyev SO, Williams JS, Jagadish C, Zou J, Li G, Titov AI (2001) Effect of ion species on the accumulation of ion-beam damage in GaN. Phys Rev B 64:035,202

L Pauling (1939) The Nature of the Chemical Bond. Cornell University Press, Ithaca, New York

Lan C, Xue JM, Wang YG, Zhang YW (2013) Molecular dynamics simulation of latent track formation in α-quartz. Chinese Physics C

Lang M, Lian J, Zhang F, Hendriks BW, Trautmann C, Neumann R, Ewing RC (2008) Fission tracks simulated by swift heavy ions at crustal pressures and temperatures. Earth and Planetary Science Letters 274:355

Lang M, Devanathan R, Toulemonde M, Trautmann C (2015) Advances in understanding of swift heavy-ion tracks in complex ceramics. Current Opinion in Solid State and Materials Science pp 39 – 48

Leach AR (2001) Molecular modelling: principles and applications, 2nd edn. Pearson Education, Harlow, England

Leino AA, Daraszewicz SL, Pakarinen OH, Nordlund K, Djurabekova F (2015) Atomistic two-temperature modelling of ion track formation in silicon dioxide. EPL 110(1):16,004, URL http://stacks.iop.org/0295-5075/110/i=1/a=16004

Lifshits IM, Kaganov MI, Tanatarov LV (1960) On the theory of radiation-induced changes in metals. J Nucl Energy Part A: Reactor Science 12:69

M E Toimil-Molares (2012) Characterization and properties of micro- and nanowires of controlled size, composition, and geometry fabricated by electrodeposition and ion-track technology. Beilstein Journal of Nanotechnology 3(1):860

Manninen M (1986) Interatomic interactions in solids: An effective-medium approach. Phys Rev B 34(12):8486

Marian J, Zepeda-Ruiz LA, Couto N, Bringa EM, Gilmer GH, Stangeby PC, Rognlien TD (2007) X. J Appl Phys 101:044,506

Matsunaga K, Fisher C, Matsubara H (2000) Tersoff Potential Parameters for Simulating Cubic Boron Carbonitrides. Jpn J Appl Phys 39:L48–L51

Medvedev N, Volkov A, Shcheblanov N, Rethfeld B (2010) Early stage of the electron kinetics in swift heavy ion tracks in dielectrics. Phys Rev B 82:125,425

Medvedev N, Rymzhanov R, Volkov A (2015a) Time resolved electron kinetics in swift heavy ion irradiated solids. Journal of Applied Physics D - Applied Physics

Medvedev N, Volkov A, Ziaja B (2015b) Electronic and atomic kinetics in solids irradiated with free-electron lasers or swift-heavy ions. Nuclear Instruments and Methods in Physics Research B 365:437 – 446

Meftah A, Brisard F, Costantini J, Dooryhee E, Hage-Ali M, Hervieu M, Stoquert J, Studer F, Toulemonde M (1994a) Track formation in sioz quartz and the thermal-spike mechanism. Physical Review B

Meftah A, Brisard F, Costantini JM, Dooryhee E, Hage-Ali M, Hervieu M, Stoquert JP, Studer F, Toulemonde M (1994b) Track formation in SiO2 quartz and the thermal-spike mechanism. Phys Rev B 49:12,457 – 12,463

Meldrum A, Zinkle SJ, Boatner LA, Ewing RC (1998) A transient liquid-like phase in the displacement cascades in zircon, hafnon and thorite. Nature 395:56–58

Miyagawa Y, Nakadate H, Djurabekova F, Nakao S, Miyagawa S (2002) Dynamic-sasamal :simulation software for high dose ion implantation. Surf&Coat Tech 158-159:87

Mookerjee S, Beuve M, Khan SA, Toulemonde M, Roy A (2008) Sensitivity of ion-induced sputtering to the radial distribution of energy transfers: A molecular dynamics study. Phys Rev B 78:045,435

Munetoh S, Motooka T, Moriguchi K, Shintani A (2007) Interatomic potential for SiO systems using Tersoff parameterization . Computational Materials Science 39(2):334 – 339

N W Lima RIGSMRSTEMB L I Gutierres, Papaléo RM (2016) Molecular dynamics simulation of polymerlike thin films irradiated by fast ions: A comparison between fene and lennard-jones potentials. Phys Rev B 94:195,417

Ni B, Lee KH, Sinnott SB (2004) A reactive empirical bond order (REBO) potential for hydrocarbon oxygen interactions. J Phys: Condens Matter 16:7261–7275

Nordlund K (1995) Molecular dynamics simulation of ion ranges in the 1 – 100 keV energy range. Comput Mater Sci 3:448

Nordlund K, Keinonen J, Kuronen A (1994) Effect of the Interatomic Si-Si-potential on Vacancy Production during Ion Implantation of Si. Physica Scripta T54:34

Nordlund K, KeinonenJ, Mattila T (1996) Formation of ion irradiation-induced small-scale defects on graphite surfaces. Phys Rev Lett 77(4):699

Nordlund K, Runeberg N, Sundholm D (1997) Repulsive interatomic potentials calculated using Hartree-Fock and density-functional theory methods. Nucl Instr Meth Phys Res B 132:45–54

Nordlund K, Ghaly M, Averback RS, Caturla M, Diaz de la Rubia T, Tarus J (1998) Defect production in collision cascades in elemental semiconductors and FCC metals. Phys Rev B 57(13):7556–7570

Nordlund K, Wallenius J, Malerba L (2005) Molecular dynamics simulations of threshold energies in Fe. Nucl Instr Meth Phys Res B 246(2):322–332

Ohta H, Hamaguchi S (2001) Classical interatomic potentials for Si-O-F and Si-O-Cl systems. J Chemical Physics 115(14):6679–90

Ojanperä A, Krasheninnikov AV, Puska M (2014) Electronic stopping power from first-principles calculations with account for core electron excitations and projectile ionization. Phys Rev B 89:035,120

Oligschleger C, Jones RO, Reimann SM, Schober HR (1996) Model interatomic potential for simulations in selenium. Phys Rev B 53:6165

Pailthorpe B, Mahon P (1990) Molecular dynamics simulation of thin film diamond. Thin Solid Films 193/194:34

Pakarinen OH, Djurabekova F, Nordlund K, Kluth P, Ridgway M (2009) Molecular dynamics simulations of the structure of latent tracks in quartz and amorphous SiO_2. Nucl Instr Meth Phys Res B 267:1456–1459

Pakarinen OH, Djurabekova F, Nordlund K (2010) Density evolution in formation of swift heavy ion tracks in insulators. Nucl Instr Meth Phys Res B 268:3163

Peltola J, Nordlund K, Keinonen J (2006) Electronic stopping power calculation method for molecular dynamics simulations using local Firsov and free electron-gas models. Rad Eff & Def in Sol 161(9):511–521

Polvi J, Luukkonen P, Nordlund K, Järvi TT, Kemper TW, Sinnott SB (2012) Primary radiation defect production in polyethylene and cellulose. J Phys Chem B 116(47):13,932

Powell D, Migliorato MA, Cullis AG (2007) Optimized Tersoff potential parameters for tetrahedrally bonded III-V semiconductors. Phys Rev B 75(11):115,202

Pronnecke S, Caro A, Victoria M, Diaz de la Rubia T, Guinan MW (1991) The effect of electronic energy loss on the dynamics of thermal spikes in Cu . J Materials Research 6(3):483–91

Pruneda JM, Sánchez-Portal D, Arnau A, Juaristi JI, Artacho E (2007) Electronic Stopping Power in LiF from First Principles. Phys Rev Lett 99:235,501, DOI 10.1103/PhysRevLett.99.235501

Pugacheva TS, Djurabekova FG, Valiev SK (1998) Effects of cascade mixing, sputtering and diffusion by high dose light ion irradiation of boron nitride. Nucl Instr Meth Phys Res B 141:99–104

Puska MJ, Nieminen RM, Manninen M (1981) Atoms embedded in an electron gas: Immersion energies. Phys Rev B 24(6):3037

R L Fleischer PBP, Walker RM (1975) Nuclear Tracks in Solids. University of California, Berkley

R L Fleischer RMW P B Price, Hubbard EL (1967) Criterion for registration in dielectric track detectors. Phys Rev 156:353

Raman S, Jurney ET, Warner JW, Kuronen A, Keinonen J, Nordlund K, Millener DJ (1994) Lifetimes in ^{15}N from gamma-ray lineshapes produced in the ^{2}H(^{14}N,$p\gamma$) and ^{14}N(thermal n, γ) reactions. Phys Rev C 50(2):682

Rethfeld B (2004) Unified model for the free-electron avalanche in laser-irradiated dielectrics. Phys Rev Lett 92(18):187,401

Rethfeld B, Rämer A, Brouwer N, Medvedev N, Osmani O (2014) Electron dynamics and energy dissipation in highly excited dielectrics. Nuclear Instruments and Methods in Physics Research B 327:78 – 88

Ridgway M, Bierschenk T, Giulian R, Afra B, Rodriguez MD, Araujo L, Byrne AP, Kirby N, Pakarinen OH, Djurabekova F, Nordlund K, Schleberger M, Osmani O, Medvedev N, Rethfeld B, Wesch W, Kluth P (2013) Track and voids in Amorphous Ge Induced by Swift Heavy-Ion Irradiation. Phys Rev Lett 110:245,502

Ruault MO, Chaumont J, Penisson JM, Bourret A (1984) High resolution and in situ investigation of defects in Bi-irradiated Si. Phil Mag A 50(5):667

Rymzhanov RA, Medvedev NA, Volkov AE (2016) Effects of model approximations of electron, hole, and photon transport in swift heavy ion tracks. Nuclear Instruments and Methods in Physics Research 388:41 – 52

Salonen E, Nordlund K, KeinonenJ, Wu CH (2001) Swift chemical sputtering of amorphous hydrogenated carbon. Phys Rev B 63:195,415

Samela J, Kotakoski J, Nordlund K, Keinonen J (2005) A quantitative and comparative study of sputtering yields in Au. Nucl Instr Meth Phys Res B 239(4):331–346

Samela J, Nordlund K, Popok VN, Campbell EEB (2008) Origin of complex impact craters on native oxide coated silicon surfaces. Phys Rev B 77:075,309

Sand AE, Dequeker J, Becquart CS, Domain C, Nordlund K (2016) Non-equilibrium properties of interatomic potentials in cascade simulations in tungsten. J Nucl Mater 470:119–127

Sandoval L, Urbassek HM (2009) Influence of electronic stopping on sputtering induced by cluster impact on metallic targets. Physical Review B 79(14)

Sastry S, Angell CA (2003) Liquid-liquid phase transition in supercooled silicon. Nature Materials 2:739

Schäfer C, Urbassek HM, Zhigilei LV (2002) X. Phys Rev B 66:115,404

Schiwietz G, Grande PL (2011) Introducing electron capture into the unitary-convolution-approximation energy-loss theory at low velocities. Phys Rev A 84:052,703, DOI 10.1103/PhysRevA.84.052703, URL http://link.aps.org/doi/10.1103/PhysRevA.84.052703

Sillanpää J, Peltola J, Nordlund K, Keinonen J, Puska MJ (2001) Electronic stopping calculated using explicit phase shift factors. Phys Rev B 63:134,113

Skupinski M, Toulemonde M, Lindeberg M, Hjort K (2005) Ion tracks developed in polyimide resist on Si wafers as template for nanowires. Nucl Instr Meth Phys Res B 240(3):681–689, DOI {10.1016/j.nimb.2005.04.128}

Stillinger FH, Weber TA (1985) Computer simulation of local order in condensed phases of silicon. Phys Rev B 31:5262

Stoller RE, Tamm A, Beland LK, Samolyuk GD, Stocks GM, Caro A, Slipchenko LV, Osetsky YN, Aabloo A, Klintenberg M, Wang Y (2016) Impact of Short-Range Forces on Defect Production from High Energy Collisions. Journal of chemical theory and computation 12(6):2871–2879

Stuart SJ, Tutein AB, Harrison JA (2000) A Reactive Potential for Hydrocarbons with Intermolecular Interactions. J Chem Phys 112:6472

Stuchbery AE, Bezakova E (1999) Thermal-Spike Lifetime from Picosecond-Duration Preequilibrium Effects in Hyperfine Magnetic Fields Following Ion Implantation. Phys Rev Lett 82(18):3637

TATombrello (1984) Track damage and erosion of insulators by ion-induced electronic processes. Nucl Inst and Meth in Phys Res B DOI https://doi.org/10.1016/0168-583X(84)90265-9

Tersoff J (1988) New Empirical approach for the structure and energy of covalent systems. Phys Rev B 37:6991

Timkó H, Djurabekova F, Costelle L, Nordlund K, Matyash K, Schneider R, Toerklep A, Arnau-Izquierdo G, Descoeudres A, Calatroni S, Taborelli M, Wuensch W (2010) Mechanism of surface modification from the arc plasma-surface interaction in Cu. Phys Rev B 81:184,109

Toulemonde M, Dufour C, Meftah A, Paumier E (2000a) Transient thermal processes in heavy ion irradiation of crystalline inorganic insulators. Nucl Instr and Meth in Phys Res B 166 – 167:903 – 912

Toulemonde M, Dufour C, Meftah A, Paunier E (2000b) Transient thermal processes in heavy ion irradiation of crystalline inorganic insulators. Nucl Instr Meth Phys Res B 166-167:903–912

Toulemonde M, Assmann W, Dufour C, Meftah A, Studer F, Trautmann C (2006) Experimental phenomena and thermal spike model description of ion tracks in amorphisable inorganic insulators. Mat Fys Medd Kong Dan Vid Selsk 52:263

Träskelin P, Salonen E, Nordlund K, Keinonen J, Wu CH (2004) Molecular dynamics simulations of CH_3 sticking on carbon surfaces, angular and energy dependence. J Nucl Mater 334(1):65

Trautmann C, Klaumünzer S, Trinkaus H (2000) Effect of Stress on Track Formation in Amorphous Iron Boron Alloy: Ion Tracks as Elastic Inclusion. Phys Rev Lett 85(17):3648

Urbassek HM, Kafemann H, Johnson R (1994) Atom ejection from a fast-ion track: A molecular-dynamics study. Phys Rev B 49(2):786

Vazquez H, Ahlgren EH, Ochedowski O, Leino AA, Mirzayev R, Kozubek R, Lebius H, Karlusic M, Jaksic M, Krasheninnikov AV, Kotakoski J, , Schleberger M, Nordlund K, Djurabekova F (2017) Creating nanoporous graphene with swift heavy ions. Carbon 114:511

Waligórski RM, Hamm RN, Katz R (1986) he radial distribution of dose around the path of a heavy ion in liquid water. Nucl Tracks Meas 11:309

Wang ZG, Dufour C, Paumier E, Toulemonde M (1994) The s_e sensitivity of metals under swift-heavy-ion irradiation: a transient thermal process. J Phys: Condens Matter 53(34):6733

Wang ZQ, Stroud D (1988) Monte Carlo studies of liquid semiconductor surfaces: Si and Ge. Phys Rev B 38(2):1384

Watanabe T, Yamasaki D, Tatsumura K, Ohdomari I (2004) X. Appl Surf Sci 234:207

Weber WJ, Zarkadoula E, Pakarinen OH, Sachan R, Chisholm MF, Liu P, Xue H, Jin K, Zhang Y (2014) Synergy of elastic and inelastic energy loss on ion track formation in srtio3. Scientific Reports 5:7726

Yi X, Sand AE, Mason DR, Kirk MA, Roberts SG, Nordlund K, Dudarev SL (2015) Direct observation of size scaling and elastic interaction between nano-scale defects in collision cascades. EPL 110:36,001

Yu JG, Sinnott SB, Phillpot SR (2007) Charge optimized many-body potential for the Si/SiO2 system. Phys Rev B 75(8):085,311

Zeb MA, Kohanoff J, Sanchez-Portal D, Arnau A, Juaristi JI, Artacho E (2012) Electronic Stopping Power in Gold: The Role of d Electrons and the H=He Anomaly. Phys Rev Lett 108:225,504

Zhigilei L, PBSKodali, BJGarrison (1998) A Microscopic View of Laser Ablation. J Chem Phys B 102:2845

Zhigilei LV, Garrison BJ (1999) Pressure waves in microscopic simulations of laser ablation. Mat Res Soc Symp Proc 538:491

Ziegler JF (????) SRIM-2013 software package, available online at *http://www.srim.org*.

Ziegler JF (1995) TRIM-95 computer code, private communication

Ziegler JF, Biersack JP, Littmark U (1985) The Stopping and Range of Ions in Matter. Pergamon, New York

Zinoviev AN, Nordlund K (2017) Comparison of repulsive interatomic potentials calculated with an all-electron DFT approach with experimental data. Nucl Instr Meth Phys Res B 406:511–517